

Carboxyphenyl Metalloporphyrins as Photosensitizers of Semiconductor Film Electrodes. A Study of the Effect of Different Central Metals

Miguel Gervaldo, Fernando Fungo, Edgardo N. Durantini, Juana J. Silber, Leonides Sereno, and Luis Otero*

Departamento de Química, Universidad Nacional de Río Cuarto, Agencia Postal Nro 3, X5804BYA Río Cuarto, Argentina

Received: July 4, 2005; In Final Form: August 24, 2005

Free-base (**P**), Zn(II) (**P_{Zn}**), Cu(II) (**P_{Cu}**), Pd(II) (**P_{Pd}**), Ni(II) (**P_{Ni}**), and Co(II) (**P_{Co}**) 5-(4-carboxyphenyl)-10,15,20-tris(4-methylphenyl) porphyrins were designed and synthesized to be employed as spectral sensitizers in photoelectrochemical cells. The dyes were studied adsorbed on SnO₂ nanocrystalline semiconductor and also in Langmuir–Blodgett film ITO electrodes in order to disclose the effect of molecular packing on the studied properties. Electron injection yields were obtained by fluorescence quenching analysis comparing with the dyes adsorbed on a SiO₂ nanocrystalline insulator. Back electron-transfer kinetics were measured by using laser flash photolysis. The unmetallized and metallized molecules have different singlet state energies, fluorescence quantum yields, and redox properties. The quantum yields of sensitized photocurrent generation are shown to be highly dependent on the identity of the central metal. It is shown that **P_{Ni}** and **P_{Co}** do not present a photoelectric effect. The other porphyrins present reproducible photocurrent, **P_{Pd}** being the one that gives the highest quantum yield even in closely packed ITO/LB films. Photocurrent quantum yields increase as the dye ground-state oxidation potential becomes more anodic, which is in agreement with the observation, obtained by laser flash photolysis, that back electron-transfer kinetics decrease with the increase in the driving force for the recombination process. This effect could be exploited as a design element in the development of new and better sensitizers for high-efficiency solar cells involving porphyrins and related dyes.

Introduction

Several large band gap metal oxide semiconductors such as TiO₂, ZnO, and SnO₂ have been spectrally sensitized by metal–organic dyes in order to extend their photoelectrochemical response to the visible region.^{1–3} The energy difference between the conduction band edge of an n-type semiconductor film and the oxidation potential of the excited sensitizer present as an adsorbate provides a driving force for excited-state heterogeneous charge injection.^{4,5} In a porous film of nanometer-sized semiconductor particles, the effective surface area can be greatly enhanced, producing substantial light absorption, even with only a monolayer of dye on each particle.⁶ As has been pointed out, there are several analogies between natural photosynthesis and dye-sensitized nanocrystalline semiconductor electrodes.^{7,8} Due to their primary participation in the photosynthesis process and properties, many studies on the development of optoelectronic and energy conversion devices incorporate chlorophyll derivatives, and several related metallized and unmetallized tetrapyrrolic compounds, as light receptors and charge storage units. Porphyrin has been often used in achieving spectral sensitization of wide band gap semiconductors,^{9–17} and this point has recently been thoroughly reviewed by Campbell et al.⁹ Light harvesting and charge separation efficiencies in a range of porphyrin dyes adsorbed on nanostructured TiO₂ were found comparable to those in natural photosynthesis, with a very high (nearly 80%) incident-photon-to-current efficiency (IPCE).⁷ However, the performance of dye-sensitized photoelectrochemical cells can be severely limited by any recombination reaction which follows

the light-driven charge separation. The factors affecting the recombination rates are the object of active investigations. A study on a series of ruthenium bipyridyl dyes, in addition to porphyrin and phthalocyanine dyes, shows that the primary factor controlling the charge recombination dynamics in dye-sensitized nanocrystalline TiO₂ films is the spatial separation of the dye cation from the electrode surface.¹⁸ On the other hand, Tachibana et al.¹⁹ showed that, with favorable energetics, electron injection proceeds on ultrafast time scales, and charge recombination rates are nearly independent of the sensitizer and rather associated with the heterogeneity of the traps in the TiO₂. They suggest that the high photocurrent efficiency obtained with a Ru(II) complex could be due to the favorable electron transfer between the iodide redox-active electrolyte (acting as a sacrificial donor) and the photooxidized dye. Nonetheless, a number of studies that used structurally related dyes showed a strong observable effect in the photoelectric yields, depending on the central metal in the organometallic complex. For example, Kuciauskas et al.²⁰ showed that osmium and ruthenium polypyridyl complexes exhibit very fast ($> 10^8$ s⁻¹) electron injection rate constants when they are adsorbed over nanocrystalline TiO₂. However, charge recombination between photoinjected electrons and the oxidized dye was observed in the nano-to-millisecond time range, with rate constants significantly larger for sensitizers having more negative reduction potentials of the oxidized dye ground state. The authors concluded that the charge recombination occurs in the Marcus inverted region, with rates decreasing with increasing driving force for the recombination process.^{20,21} The observation of the inverted region in dye-sensitized solar cell recombination processes implies that the improvement of

* To whom correspondence should be addressed. E-mail: lotero@exa.unrc.edu.ar.

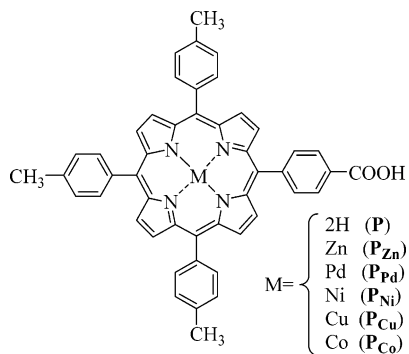


Figure 1. Structures of the sensitizing dyes.

cell performance could be reached through the use of dyes with electronic coupling that favor sensitizer regeneration relative to charge recombination. Dang and Hupp also reported direct observation of Marcus-type inverted electron transfer in SnO_2 -dye systems.²²

Because porphyrins are particularly attractive as light harvesters, we designed and synthesized a series of metallo 5-(4-carboxyphenyl)-10,15,20-tris(4-methylphenyl) porphyrins, with $M = 2\text{H}$ (**P**), Zn(II) (**P_{Zn}**), Cu(II) (**P_{Cu}**), Pd(II) (**P_{Pd}**), Ni(II) (**P_{Ni}**), and Co(II) (**P_{Co}**) (Figure 1), to analyze the effect of the metal substitution in the quantum yield generation of photoelectric effects by the dyes as photosensitizers of SnO_2 nanocrystalline semiconductor film electrodes. Electron injection yields were measured through fluorescence quenching analysis and back electron-transfer kinetics by laser flash photolysis. In addition, to assess the effect of molecular packing of the dyes, photocurrent generation from Langmuir–Blodgett films of the dyes over ITO electrodes was studied. The metallized and unmetallized molecules have different singlet state energies, fluorescence quantum yields, and redox properties²³ and bear a carboxylic acid group in order to benefit the adsorption and electronic coupling of the sensitizer with the basic semiconductor oxide electrode^{24,25} and the orientation at the air–water interface in the Langmuir–Blodgett film formation.

Experimental Section

General. The voltammetric characterization of the redox process for the porphyrin dyes was acquired with a potentiostat–galvanostat Autolab (Electrochemical Instruments) using a Pt disk working electrode of 0.204 cm^2 and a Pt counter electrode in a conventional three-compartment Pyrex cell. A freshly prepared Ag/AgCl quasi-reference electrode was used. The working electrode was cleaned between each experiment by polishing with $0.3\text{ }\mu\text{m}$ alumina paste, followed by solvent rinses. Studies were carried out in N_2 -degassed dichloromethane (DCM) with 0.1 M tetrabutylammonium hexafluorophosphate (TBAHF₆) supporting electrolyte. The voltammograms were corrected for IR drop by the positive feedback technique. After each voltammetric experiment, ferrocene was added, and the potential axis was calibrated against the formal potential for the ferrocene/ferrocene redox couple.²⁶ The oxidation potentials of the dye-excited state (E^*_{ox}) were estimated by subtracting the excitation energy from the redox potentials of the molecule in the ground state.

Absorption spectra were recorded on a Shimadzu UV-2401PC spectrophotometer. Fluorescence spectra were recorded on a Spex FluoroMax fluorimeter. Mass spectra were taken with a Varian Matt 312 operating in EI mode at 70 eV . The light-harvesting efficiency (LHE) of the dye adsorbed over the photoelectrode was obtained from $\text{LHE} = 1 - 10^{-A}$, where A is the monochromatic absorbance.

Porphyrins. 5-(4-Carboxyphenyl)-10,15,20-tris(4-methylphenyl) porphyrin (**P**) and its complexes with Zn(II) (**P_{Zn}**), Pd(II) (**P_{Pd}**), Cu(II) (**P_{Cu}**), and Ni(II) (**P_{Ni}**) were synthesized as previously described.^{11,27} Cobalt(II) 5-(4-carboxyphenyl)-10,15,20-tris(4-methylphenyl) porphyrin (**P_{Co}**) was synthesized by refluxing a mixture of **P** (15 mg, 0.021 mmol) in 30 mL of chloroform with a saturated solution of cobalt(II) acetate in methanol (2 mL) for 2 h. Solvents were evaporated under reduced pressure, and flash chromatography (silica gel, dichloromethane/methanol 10%) yielded 15 mg (94%) of **P_{Co}**. MS m/z 757 (M^+) (757.2014 calcd for $\text{C}_{48}\text{H}_{34}\text{N}_4\text{O}_2\text{Co}$).

Preparation of Nanocrystalline Films. The SnO_2 nanostructured thin film electrodes were prepared using an already described method.¹² As base contact optically transparent electrodes of indium tin oxide (ITO, $100\text{ }\Omega/\text{square}$, Delta Technologies) were used. ITO/ SnO_2 electrodes were prepared by spin coating using a P6204-A model specialty coating system. The final films were annealed at $450\text{ }^\circ\text{C}$ for 1 h. The SnO_2 films were analyzed by X-ray diffractometry (Siemens D5000, $\text{Cu K}\alpha$ radiation, XRD) and atomic force microscopy (Nano-scope III, AFM) in order to assess the crystallinity of the sample.¹³ SiO_2 nanostructured films were formed with the same procedure as that used for SnO_2 photoelectrodes, using a SiO_2 colloidal suspension in water (Ludox SM 30).

ITO/ SnO_2 electrodes were modified with dyes by soaking ITO/ SnO_2 films in a saturated n -hexane/DCM 80/20 solution of the corresponding dye. The electrodes were then washed with the same solvent, dried under a N_2 stream at room temperature, and stored in vials. A copper wire was connected to the electrode's surface with an indium solder to achieve electrical contact.

Photoelectrochemistry. Unless other conditions are indicated, photoelectrochemical experiments were conducted in aqueous solutions (0.01 M) of hydroquinone (H_2Q , recrystallized from toluene), with phosphate buffer (pH = 5.2) prepared from 0.05 M NaH_2PO_4 and NaOH . These solutions were degassed by bubbling Ar and maintaining a continuous stream on the top of the cell. A strong effect on the charge collection efficiency in porphyrin-derivatized TiO_2 photoelectrodes with electrolyte pH was observed, mainly due to oxide surface protonation;²⁸ consequently, special care was taken to control the pH. The measurements were carried out under potential control in an already described quartz photoelectrochemical cell¹³ equipped with a Ag/AgCl reference electrode, and a Pt foil auxiliary electrode, using a computer-controlled battery-operated low-noise potentiostat (Palm Sens). Action spectra were obtained by illumination of the photoelectrodes with monochromatic light obtained from a 75 W high-pressure Xe lamp (Photon Technology Instrument, PTI) and a computer-controlled PTI high-intensity grating monochromator (5 nm band wide). The steady-state photocurrents were obtained in front face configuration (illuminated area: 1 cm^2). The incident light intensities at different wavelengths were measured with a Coherent Laser-Mate Q radiometer (sensitivity $1\text{ }\mu\text{W}$). Transient photocurrents were generated by laser pulses (vide infra) at different applied potential bias (M5 LYP Electronica Argentina potentiostat), and current output signal of the potentiostat was coupled to a digital oscilloscope.

Langmuir–Blodgett (LB) Film Preparation. Monolayers were prepared on a model 610 Nima Langmuir–Blodgett trough placed in a dark box. The subphase was ultrapure water (from LABCONCO equipment model 90901-01) with phosphate buffer (pH = 5.2). This pH value was selected because it is the same as that at which the photoelectrochemical experiments

were carried out. The temperature was maintained at 25 ± 0.5 °C. Porphyrins films at the water–air interface were formed by applying a drop of a suitable dye solution (ca. $1-2 \times 10^{-3}$ M in chloroform) on the clean subphase by microsyringe. The chloroform was allowed to evaporate for 15 min, and the monolayer was then compressed. The substrates for monolayer depositions were ITO-coated borosilicate glass made hydrophilic by immersing them in 0.1 M NaOH solution for 30 min and then thoroughly rinsing them with ultrapure water. The clean ITO slide was immersed in the subphase, and the monolayer was formed at the air–water interface and compressed at 50 cm^2/min . The monolayers were transferred, at a constant surface pressure of 25 mN/m , to the slides by the vertical transfer method at 25 mm/min . Only films having transfer ratios of 1.0 ± 0.1 were used in the experiments. A copper wire was connected to the electrode's surface with an indium solder to achieve electrical contact.

Laser Flash Photolysis Experiments. The laser flash photolysis setup has been described elsewhere.²⁹ A Q-switched Nd:YAG laser (Spectron SL400) was used as the excitation source operating at 532 nm (20 ns half-width) in order to excite the porphyrin compounds adsorbed over ITO/SnO₂ electrodes placed in the already described photoelectrochemical cell. It has been reported that the electron injection kinetics into the semiconductor are rather insensitive to experimental conditions.¹⁹ By contrast, the recombination kinetics between the dye cation and the photoinjected electrons are strongly dependent upon experimental conditions, with variation in the recombination rate from picoseconds to milliseconds depending upon the excitation intensity, solvent/electrolyte composition, and applied electrical bias.^{19,30} In order to compare between the different sensitizer dyes, considerable care was taken to minimize such experimental variation. The applied potential on the ITO/SnO₂/dye electrodes was kept under control in a three-electrode configuration, in Ar-degassed phosphate buffer solutions without sacrificial donor hydroquinone. The laser beam was abated by using neutral filters in order to avoid photodegradation of the samples. The output of the detector was coupled to a digital oscilloscope (Hewlett-Packard HP-54504A). About 20 shots were usually needed for averaging decay times, to get a good signal-to-noise ratio. The averaged signals were analyzed as multiple exponential decays by using calculation software.

Results and Discussion

Electrochemistry. Cyclic voltammetry was used in order to evaluate the redox properties of the dyes. Usually, porphyrins show two well-defined reversible single-electron oxidations in nonbinding solvent,³¹ corresponding to ring oxidation and formation of the radical cation and dication, respectively.²³ Figure 2 shows typical oxidation voltammograms for all the studied porphyrins. In metalloporphyrins the ring or metal-centered oxidations are determined by various factors, including the intrinsic redox potentials of the porphyrin ring and metal center, the number and type of ligands on the metal ion, and the properties of the solvent. In the case of Zn(II), Cu(II), and Pd(II) tetraphenyl porphyrins (M(II)TPP) it has been established that the first anodic process involves porphyrin macrocycle oxidation and the formation of $[\text{M}(\text{II})(\text{TTP})]^+$.^{23,31} On the other hand, it is known that in the case of several Co(II) porphyrins the electrochemistry is dominated by the metal-centered reaction, the most common of which involves the Co(II)/Co(III) process, which usually occur at less anodic potentials than macrocycle oxidation.³² In agreement with this, in our case the anodic scan of **P**_{Co} (Figure 2c) shows three voltammetric waves, in which

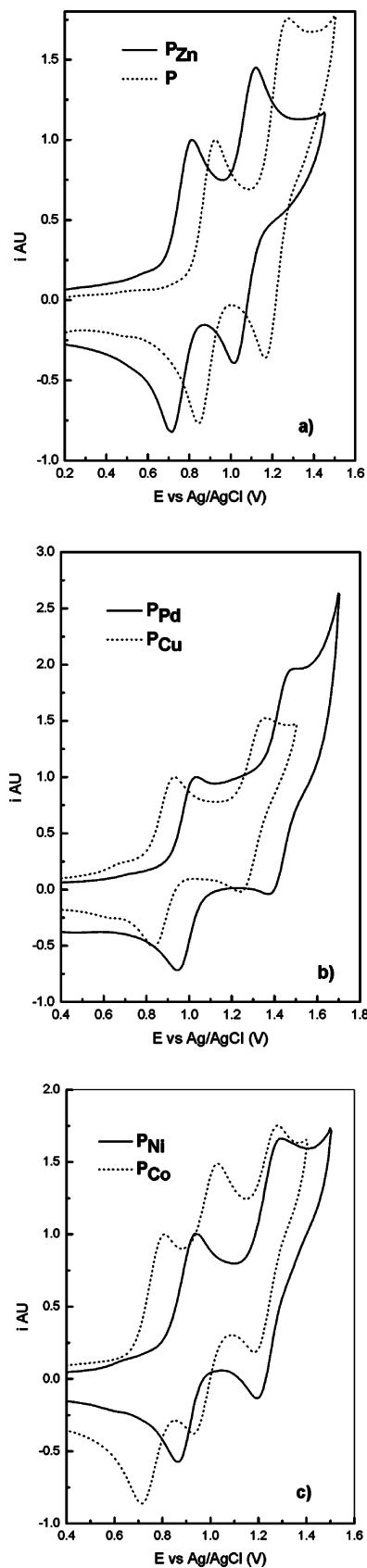


Figure 2. Cyclic voltammograms of (a) **P**, **P**_{Zn}, (b) **P**_{Pd}, **P**_{Cu}, and (c) **P**_{Ni}, **P**_{Co} at a platinum electrode in DCM containing 0.1 M TBAHFP as supporting electrolyte; sweep rate = 0.100 V/s. The currents have been normalized to one at the first oxidation wave for comparison.

the one at lower potential corresponds to the central metal, Co(II), oxidation and the other two to oxidations of the porphyrin-ring system. On the other hand, nickel porphyrin electrochem-

TABLE 1: Electrochemical, LB, and Spectroscopic Properties of Dyes

dye	E_{ox}^a	area/ molecule ^b	λ_{max} DCM ^c	λ_{max} SnO ₂ /dye ^c	λ_{max} LB ^c
P _{Zn}	0.76	50	425	434	438
P	0.88	52	421	431	427
P _{Cu}	0.87	63	419	421	429
P _{Pd}	1.04	90	419	427	427
P _{Ni}	0.89		419	425	
P _{Co}	0.75		412	430	

^a First oxidation potential of dyes (V vs SCE). ^b LB films (\AA^2).
^c Soret band (nm).

istry has shown some degree of controversy in the past.³¹ Seth et al.³³ made a careful revision of Ni(II)TPP oxidation, where the resonance Raman and EPR spectra of the one-electron oxidation products were examined in detail. They concluded that the limiting case forms $[\text{Ni(III)TPP}]^+$ and $[\text{Ni(II)TPP}]^+ \cdot$ do not accurately describe the ground states of the oxidation products of Ni(II)TPP, and an equilibrium exists between the electrochemically generated Ni(II) porphyrin's cation radical and Ni(III) porphyrins. Additionally, more recently Kadish et al.³⁴ reported the electrochemistry studies of 29 different nickel porphyrins in dry DCM and confirmed that in all cases it was the porphyrin macrocycle and not the nickel atom that was oxidized under their electrochemical experimental conditions (DCM, 0.1 M tetra *n*-butylammonium perchlorate or 0.1 M tetra *n*-butylammonium hexafluorophosphate). In similar conditions, we observed two oxidation waves in the anodic scan of P_{Ni} (Figure 2c) which is consistent with those results.³⁴

Table 1 summarizes the redox potentials for the first oxidation process of each investigated dye, calculated using the expression $(E_p \text{ forward} - E_p \text{ backward})/2$. The values are consistent with the effect of the peripheral substitution of the methyl and carboxyl groups (Figure 1). It is known that peripheral substitution in para-substituted tetraphenylporphyrin $[\text{H}_2(p\text{-X)TPP}]^{35}$ and metalloporphyrins^{36–38} ($[\text{M}(p\text{-X)TPP}]$ where $\text{M} = \text{Mn}^{2+}, \text{Fe}^{2+}, \text{Co}^{2+}, \text{Ni}^{2+}, \text{Cu}^{2+},$ and Zn^{2+}) has an effect in modulating their electron donor–acceptor capabilities. In our case, we observed that the dye oxidation potentials are less anodic than the values reported for the tetraphenylporphyrins without a substituent,³¹ which is evidence that the electron donor effect characteristic of the three methyl groups prevails over the single carboxylic group electron acceptor effect. Aside from this effect for P, P_{Zn}, P_{Pd}, P_{Ni}, and P_{Cu}, where ring oxidation produces the porphyrin radical cation, the change in the redox potential with different metal substitution follows the same order as that already reported for M(II)TPP,³¹ that is, that P_{Zn} has the lowest and P_{Pd} the highest.

LB Film Properties. It is known that unsubstituted *meso*-tetraphenylporphyrins do not form stable monolayer films in pure form at gas–liquid interfaces.³⁹ However, 5-(4-carboxyphenyl)-10,15,20-tris(4-methylphenyl) porphyrins exhibit well-behaved monomolecular films at an air–water interface, in which the carboxylic group of the dye is assumed to be oriented into the water.⁴⁰ The photoelectrochemical response of the LB monolayer over ITO was analyzed only for the dyes that showed photocurrent generation on ITO/SnO₂/dye electrodes (vide infra).

In the compressed monolayers the molecules appear to be oriented so that the plane of the ring is perpendicular to the surface, as can be deduced from the average area per molecule of porphyrins at the air–water interface, which was determined by extrapolating the linear region of the surface pressure versus area isotherms to zero pressure (Figure 3). The observed molecular areas for the monolayers of the compounds are

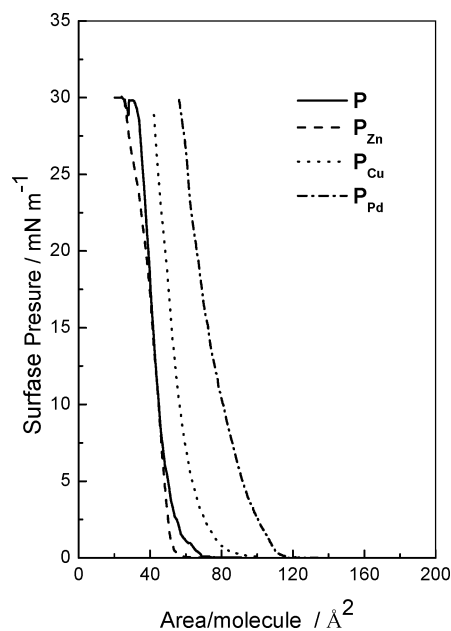


Figure 3. Surface pressure–area isotherm of porphyrin dye films at the air–water interface. Subphase: 0.05 M phosphate buffer, pH = 5.2.

gathered in Table 1. If the dyes lie with the porphyrin ring being parallel to the air–water interface, the occupied area per molecule should be at least $\approx 360 \text{ \AA}^2$, as can be inferred from the calculated molecular geometry (AM1) for the P porphyrin. A similar observation was reported by Ogi et al.,⁴¹ who, based on their single-crystal structure, assumed 220 \AA^2 as the in-plane area for TPP. As can be observed in Table 1, the areas are quite smaller than those calculated, and consequently, it can be assumed that the molecules assemble perpendicular to the subphase plane, leaving dye monolayers with typical absorbance, at the Soret band, of ≈ 0.06 for all porphyrins.

Absorption Spectroscopy. The electronic spectra of porphyrins were recorded in DCM solution and compared to those of the porphyrin adsorbed onto thin ITO/SnO₂ films and deposited as ITO/LB monolayers. The absorption spectra of the dyes in solution show a series of visible bands due to $\pi\text{--}\pi^*$ transitions of the conjugated macrocycle.⁴² In the ITO/SnO₂/dye adsorbed films the Soret and Q-bands show similar electronic transitions to those observed for monomeric absorption in DCM, but the bands are broader and are shifted to longer wavelengths in comparison with those in solution (Figure 4 and Table 1). This may be caused by the interaction of the porphyrins with the polar surface of the electrode, as well as the possible formation of porphyrin aggregates on the surface.¹² The absorption spectra of ITO/LB films can help to clarify this point. In fact, the absorption spectra of these porphyrin LB monolayers are also broadened relative to the solution, and the Soret bands are red shifted. Choudhury et al.⁴³ found an excellent linear correlation between the red shift and the area per molecule for a series of surfactant porphyrin LB monolayers and also showed that the trend of the spectral properties of the model porphyrin compounds was not changed substantially by changing the substrate from quartz to a SnO₂-coated glass plate. Hence, they concluded that, except for monolayer disorder, no additional effect is experienced by porphyrin compounds when they are deposited onto a SnO₂ surface.⁴³ On the basis of these antecedents and our experimental results, we can conclude that the red shift observed in the ITO/SnO₂/dye adsorbed films is due, at least in part, to the close packing of the porphyrin onto the electrode. Since this can drive to self-quenching of the

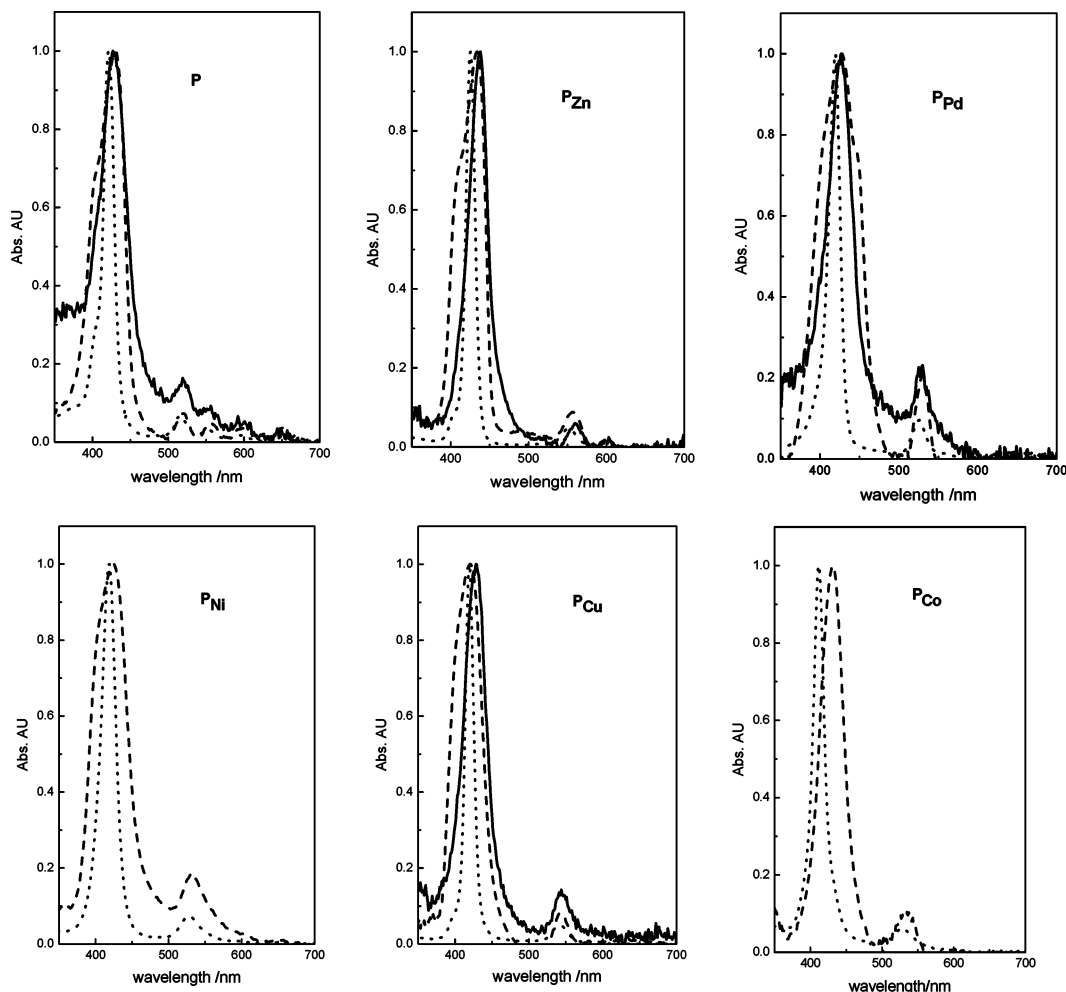


Figure 4. Absorption spectra of porphyrins: DCM solution (dotted line), in the adsorbed state over ITO/SnO₂/electrodes (dashed line), and Langmuir-Blodgett films (solid line). The absorbance has been normalized to one at the Soret band for comparison.

porphyrin excited state,⁴⁴ in the photoelectrochemical studies we kept similar and low dye coverage for the different studied porphyrins. For ITO/SnO₂ electrodes constructed as described in the Experimental Section, we found that the maximum porphyrin dye coverage ($\Theta = 1$) produces absorbance around 1.0–1.2 in the Soret band. Therefore, electrodes with absorbance of ≈ 0.2 were used.

Fluorescence Spectroscopy. **P** and **P_{Zn}** show observable fluorescence, both in solution and adsorbed on ITO/SnO₂/dye electrodes; however, the emission intensities for the other porphyrins are much lower in solution, and no emission was detected in adsorbed state. Thus, electron injection yields measured through fluorescence quenching in ITO/SnO₂/dye electrodes were analyzed for **P** and **P_{Zn}**. Figure 5a shows the absorption-corrected fluorescence spectra of the dyes in toluene solution. The **P_{Zn}** has two maxima at 604 and 652 nm, whereas for **P** they are at 653 and 719 nm. On the other hand, fluorescence intensity of the dyes adsorbed over the ITO/SnO₂ film is much smaller than the same over the insulator ITO/SiO₂ (Figure 5b). In other words, an additional quenching pathway seems to be effective when the dyes are adsorbed on the semiconductor surface. This quenching can be interpreted in terms of electron transfer from the excited dye to the semiconductor. After production of the excited state by photon absorption, several deactivation pathways are possible: radiative relaxation, thermal (nonradiative) relaxation, or interfacial charge injection. When the latter occurs an external circuit could collect the injected electrons, producing an observable photocurrent.

In contrast, when the dye is adsorbed on ITO/SiO₂ (band gap = 6.9 eV),⁴⁵ the oxidation potential of the dye-excited state (E_{ox}^*) lies at much lower energy than the conduction band edge of the insulator. Consequently, electron transfer is not possible, and the fluorescence is not affected by this additional mechanism. For a dye adsorbed on ITO/SnO₂ there is a driving force for photoinduced electron transfer from the dye to the semiconductor, defined as $\Delta E = -e(E_{ox}^* - E_{FB})$,⁴⁶ where E_{FB} is the potential of the semiconductor flat band (~ -0.02 V vs NHE)⁴⁷ and e is the electronic charge. Since electron transfer is in competition with radiative and nonradiative processes, one can express the charge injection yield (Φ_{inj}) from the excited dye to the semiconductor as shown in eq 1.^{13,48}

$$\Phi_{inj} = \frac{I_f(0) - I_f(e)}{I_f(0)} \quad (1)$$

where $I_f(0)$ and $I_f(e)$ are the fluorescence intensity in the absence and in the presence of charge-transfer respectively, obtained from the area below the corrected emission spectra of the photoelectrodes (Figure 5b). Under our experimental conditions the electron injection efficiency was found to be similar for both **P_{Zn}** and **P** porphyrins with $\Phi_{inj} \approx 0.9$.

Photoelectrochemistry. Upon excitation of ITO/SnO₂/dye electrodes anodic photocurrents and negative open-circuit photopotentials are generated in the case of **P_{Pd}**, **P_{Cu}**, **P_{Zn}**, and **P**, indicating that the electrons flow from the solution to ITO base contact through the illuminated electrode. On the other hand,

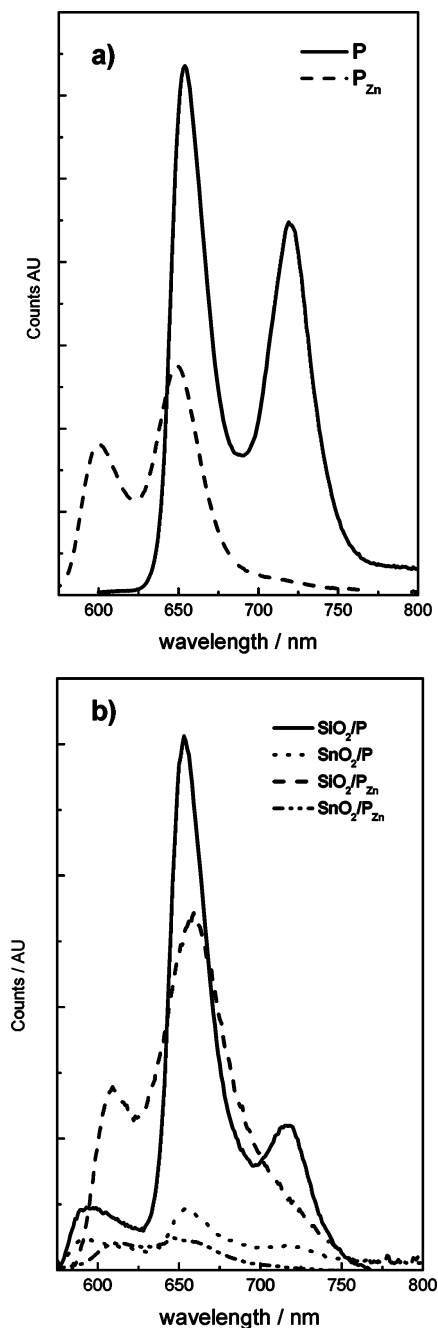


Figure 5. (a) Corrected fluorescence emission spectrum in toluene solution of P_{Zn} and P ; $\lambda_{ex} = 550$ nm. (b) Fluorescence emission spectrum of P_{Zn} and P adsorbed on SiO_2 and SnO_2 ; $\lambda_{ex} = 420$ nm. All the emission spectra were corrected by the absorbance and instrumental response.

P_{Ni} and P_{Co} show none or extremely low photoelectric effect. The lack of dye-sensitized photocurrent on large band gap semiconductor electrodes could be due to several reasons, such as inefficient electron injection, fast back electron transfer, and/or inefficient regeneration of the reduced dye ground state by the sacrificial donor.^{49–52}

It has been reported that Ni(II) porphyrin's excited state has a very short lifetime due to the π and d orbital interactions.⁵³ Soret and Q-band photoexcitation rapidly form a metal-centered (d,d^*) state. Rodriguez et al.^{54,55} showed that common Ni(II) porphyrins undergo $\pi^* \rightarrow d^*$ crossing within 1 ps, generating a porphyrin molecule with a ground-state system and an excited metal center. The d^* state repopulates the ground state with a lifetime of around 300 ps. Zamyatin et al.⁵³ reported for Ni-

(II)TPP that excitation at 400 nm converts the porphyrin system into the $S_2(\pi,\pi^*)$ state, which produced the $S_1(\pi,\pi^*)$ state in a few femtoseconds, and the $S_1(\pi,\pi^*)$ state decays to the metal-centered excited state (d,d^*) with $\tau = 0.6$ ps, which decays to the S_0 ground state with $\tau = 4–10$ ps. On the other hand, Yu et al.⁵⁶ have shown that deactivation of the Co(II)TPP S_1 state occurs through the formation of intramolecular electron transfer from the porphyrin ring to the metal center, with charge separation and recombination processes of 1.8 and 16 ps, respectively. However, it has been reported for several dyes, including porphyrins,⁵⁷ that the primary step of electron injection across the sensitizer–semiconductor interface is extremely fast in the case of a TiO_2 semiconductor (<100 fs for tetracarboxyphenyl porphyrins).¹⁹ In addition, Benkö et al.⁵⁸ demonstrated that the time constant and overall quantum yield of electron injection from RuN3 dye are similar for both TiO_2 and SnO_2 semiconductors, and the authors concluded that the electron injection process is almost independent of the semiconductor used. Moreover, the oxidation potentials of the dye-excited states (E_{ox}^*) used in this work lie at higher energy than the conduction band edge of the SnO_2 . Thus, it is possible that, although having a short lifetime, P_{Ni} and P_{Co} excited states undergo heterogeneous photoinduced electron transfer to the semiconductor. If this is the case, back electron transfer must compete quite efficiently with regeneration of the reduced dye ground state by the sacrificial donor.

For the P_{Pd} , P_{Cu} , P_{Zn} , and P porphyrins photocurrents are reproducible under several (hundreds) repeated on–off illumination cycles. Action spectra of ITO/ SnO_2 /dye and ITO/dye LB electrodes (measured under potentiostatic control) closely match the absorption spectrum of the adsorbed organic molecules in every case, as is shown in Figure 6a–d.

Monochromatic photocurrent quantum yield, expressed as the charge injection yield (Φ_{inj}) from the excited dye to the semiconductor times the charge collection efficiency (η_c) of the system, was evaluated from eq 2.⁵⁹

$$\Phi_{inj}\eta_c = IPCE/LHE \quad (2)$$

where IPCE is the incident-photon-to-photocurrent efficiency evaluated from:⁵⁹

$$IPCE = (i_{sc}1240)/(I_{inc}\lambda) \quad (3)$$

i_{sc} is the short-circuit photocurrent ($A\ cm^{-2}$), I_{inc} is the incident light intensity ($W\ cm^{-2}$), λ is the excitation wavelength (nm), and LHE is the light-harvesting efficiency (see the Experimental Section). The dependence of the photocurrent quantum yield ($\Phi_{inj}\eta_c$) on the applied potential has shown that recombination rates between photoinjected electrons and a dye cation increase as more negative potentials are applied to the semiconductor.^{20,30,50} Lower cell efficiencies at negative bias correlate with this increase in the charge recombination rate, which involves the level of the steady-state trap occupancy in the nanostructured semiconductor.⁵⁰ Thus, the effect of the bias was analyzed by recording the transient photocurrents obtained after a 532 nm laser pulse at different applied potentials (Figure 7a). As can be observed, the transient photocurrents generated by an ITO/ SnO_2 / P_{Zn} electrode increase as the applied potential becomes more anodic. This effect was observed with all the porphyrins and is mainly due to the increase in the collection efficiency of the injected electrons. Consequently, for the comparative analysis on the efficiency of the different dyes used in this work, the measurements were carried out under potential control.

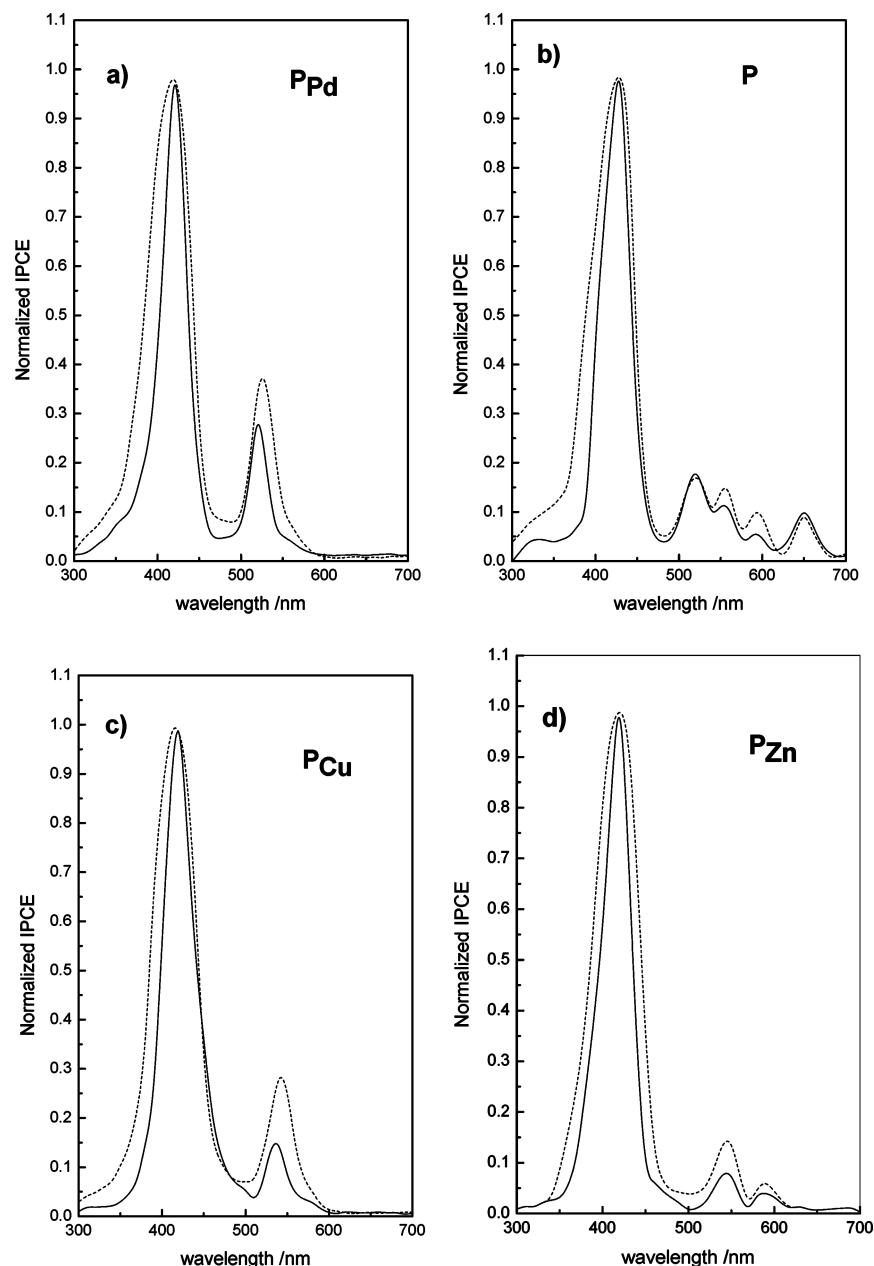


Figure 6. Photocurrent action spectra, IPCE of ITO/SnO₂/dye electrodes (---) and Langmuir–Blodgett films (—) modified with **P**, **P_{Pd}**, **P_{Cu}**, and **P_{Zn}**. H₂Q 0.01 M in phosphate buffer. Applied bias potential = 0.05 V vs Ag/AgCl.

The effect of the applied potential on the observed stationary photocurrent quantum yield expressed as the $\Phi_{inj}\eta_c$ value of the systems at the Soret bands is shown in Figure 7b for different ITO/SnO₂/dye electrodes. This experiment allows a comparative analysis of photoelectric generation efficiency of the different dyes under similar experimental conditions. $\Phi_{inj}\eta_c$ increases with the anodic bias in all cases, and Figure 7b also shows that the photocurrent quantum yield is higher in the **P_{Pd}** molecule than for the other dyes in the range of applied potential studied. Table 2 summarizes the results of the product $\Phi_{inj}\eta_c$ for the four dyes at the Soret band.

On the other hand, as was already mentioned, dye aggregation onto the electrode can drive to self-quenching of the excited state of the porphyrin in the photocurrent generation process. For example, an enhancement of photocurrent quantum yield on diluting monolayers of surfactant porphyrins with dioleoylphosphatidylcholine has been observed.^{43,60} Thus the photoelectric properties of Langmuir–Blodgett films of **P** and **P_M** used in this work, deposited on ITO electrodes, were

analyzed with the same procedure as that used in nanostructured films, to study the possible effects of the closer molecular packing and intermolecular interactions in the ultrathin layer. As can be observed in Table 2, the photocurrent quantum yield of the LB film electrodes are lower than those obtained with the nanostructured material for the same porphyrin. This could be interpreted as resulting from the aggregate mediated quenching, which diminishes interfacial isoenergetic electron transfer, and hence makes lower the photocurrent quantum yield. However, deposition of dyes over the highly doped oxide semiconductor in the ITO/LB films electrodes instead of nanostructured SnO₂ also affects the photocurrent generation process, through changes in the kinetics of the involved stages. Nevertheless, as can be seen in Table 2, the **P_{Pd}** porphyrin was shown to be the most effective sensitizer in both systems (ITO/LB films and ITO/SnO₂ electrodes). The reason for this efficiency could be related to the kinetics of the different steps in the spectral sensitization process. As shown before, the electron injection efficiency is high and similar for **P** and **P_{Zn}**

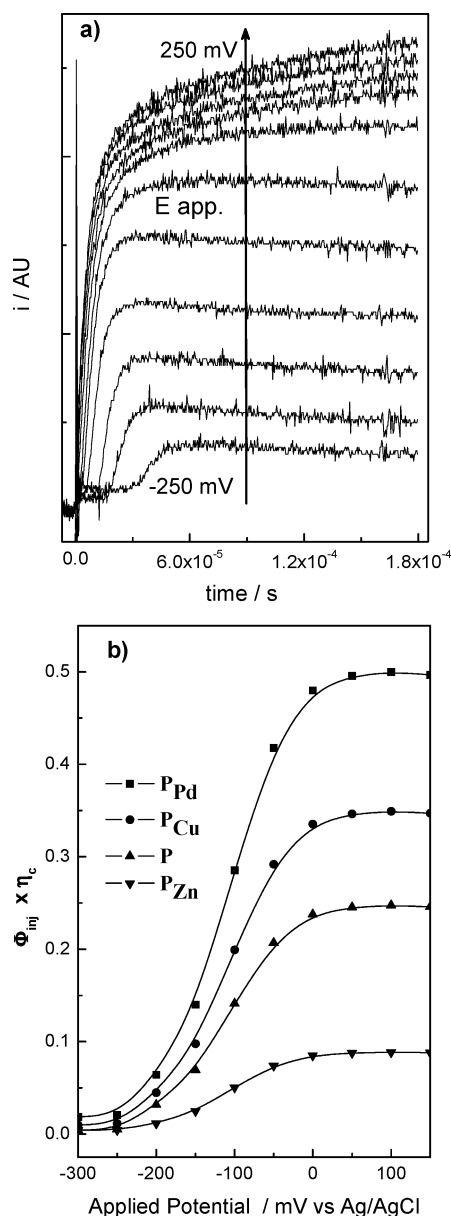


Figure 7. (a) Transient photocurrent generated by P_{Zn} dye on ITO/SnO₂/electrodes after a laser pulse ($\lambda_{exc} = 532$ nm) at different applied bias potentials. H₂Q 0.01 M in phosphate buffer. The arrow indicates the increase of anodic bias. (b) Dependence of $\Phi_{inj}\eta_c$ at the maximum of the Soret bands of ITO/SnO₂/dye electrodes on applied bias. H₂Q 0.01 M in phosphate buffer.

TABLE 2: Photoelectrochemical Properties of Dyes

dye	$\Phi_{inj}\eta_c$ ITO/SnO ₂ /dye ^a	$\Phi_{inj}\eta_c$ ITO/LB/dye ^a	$k_b \times 10^6$ s ⁻¹ b
P_{Zn}	0.10	0.007	8.13 (0.72)
			0.25 (0.27)
P	0.25	0.040	4.79 (0.79)
			0.17 (0.21)
P_{Cu}	0.35	0.028	2.23 (0.65)
			0.11 (0.34)
P_{Pd}	0.49	0.126	1.66 (0.66)
			0.14 (0.32)

^a Maximum $\Phi_{inj}\eta_c$ at Soret bands under bias voltage ($V = 0.05$ V vs Ag/AgCl; H₂Q 0.01 M). The values are an average for more than 20 electrodes for each dye. ^b Back electron-transfer kinetics fitted by a biexponential function; in parentheses, relative amplitudes (bias voltage = 0.05 V vs Ag/AgCl).

porphyrins. Thus, low charge collection efficiency of the ITO/SnO₂/ P_{Zn} system could be the limiting factor in photocurrent

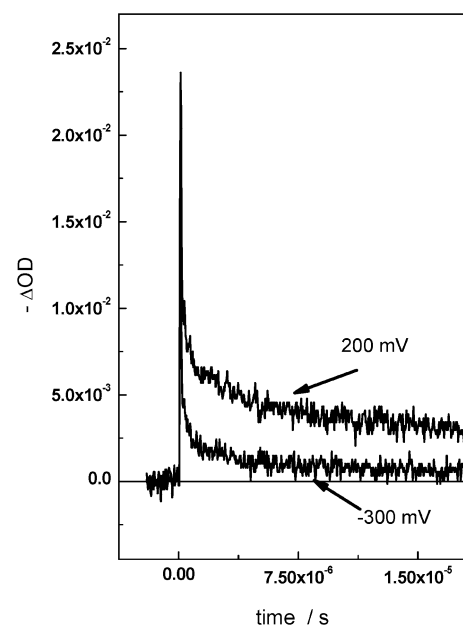


Figure 8. Kinetics of the dye ground-state recovery on ITO/SnO₂/ P_{Zn} followed at 430 nm after a laser pulse in phosphate buffer solution without H₂Q. The arrow indicates the bias potential vs Ag/AgCl.

generation through back electron transfer (i.e., the charge recombination between the photoinjected electron and the porphyrin cation).

Laser Flash Photolysis. To analyze the back electron-transfer kinetics, we examined the changes in the absorbance, measured at the dye's Soret band, following excitation after a 3.0 mJ cm⁻² laser pulse at 532 nm for ITO/SnO₂/dye electrodes. Figure 8 shows the transients in an ITO/SnO₂/ P_{Zn} electrode at different applied potentials. Electron injection results in fast bleaching followed by regeneration of the ground-state absorbance of the porphyrin compounds. As has been mentioned, in several dyes, including porphyrins,^{19,57} the primary step of electron injection across the sensitizer–semiconductor interface is fast and almost independent of the semiconductor used.⁵⁸ The recovery processes, in the absence of sacrificial donor hydroquinone, are associated with the reduction of the oxidized species formed after excitation and electron injection and are dependent on applied potential. In agreement with the observed effect on stationary and transients photocurrents, back electron transfer increases as the applied potential becomes more cathodic and reaches a nearly constant value at an anodic applied potential higher than 0.2 V vs Ag/AgCl. The regeneration process, which occurs by recombination between a photoinjected electron in the semiconductor and the oxidized dye, presents a comparatively fast step followed by a slower one, showing a complex kinetics^{49,50} attributed to multiple electrons trapping in surface defects, which affect the recovery process.^{51,52} In the kinetic analysis (Table 2) we assumed pseudo-first-order kinetics, fitted by a biexponential function, but it is known that the back electron-transfer process is a very complex phenomenon,⁵⁰ and an analysis of the relation between k_b and the photocurrent quantum yield should be taken as semiquantitative. Moreover, it has been reported³⁰ that a proportion of charge recombination occurs on time scales less than the time resolution of our laser flash photolysis setup. On the other hand, as has already been pointed out by Boschloo and Hagfeldt,⁶¹ in practice rather high laser pulse intensities are needed in order to obtain sufficient signal in laser flash photolysis experiments on dye-sensitized semiconductor electrodes, making a direct comparison with conditions that exist under normal illumination slightly difficult.

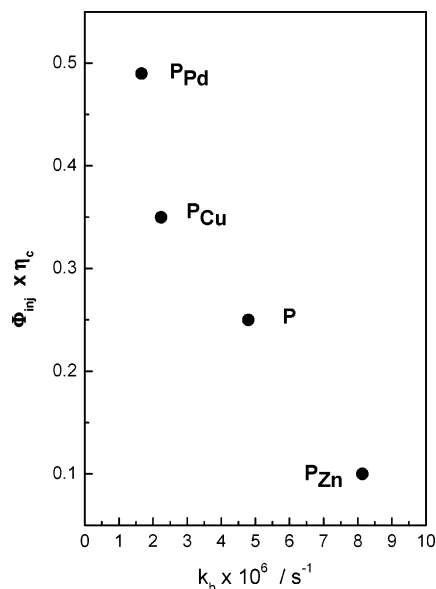


Figure 9. Dependence of $\Phi_{inj}\eta_c$ at the maximum of the Soret bands of ITO/SnO₂/dye electrodes (H₂Q 0.01 M in phosphate buffer, voltage = 0.05 V vs Ag/AgCl) on the component with the larger relative amplitude of the back electron rate constant.

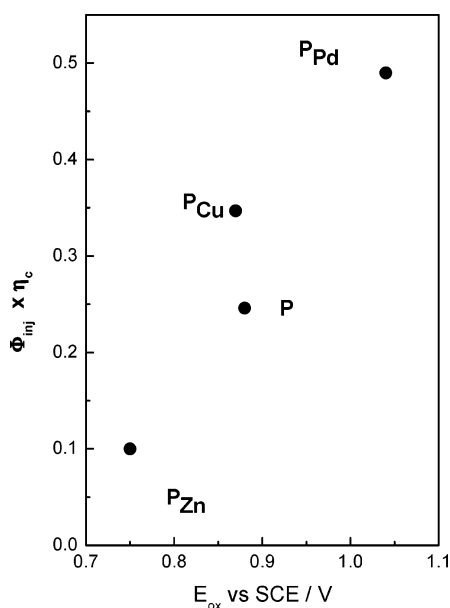


Figure 10. Dependence of $\Phi_{inj}\eta_c$ at the same conditions that those in Figure 9 of ITO/SnO₂/dye electrodes on the ground-state dye's oxidation potential.

Nevertheless, as can be observed in Figure 9, back electron transfer is faster in the case of the ITO/SnO₂/P_{Zn} electrode and decreases as the dye ground-state oxidation potential becomes more anodic, with rates decreasing with increasing driving force for the recombination process.

We found that, under our experimental conditions, photocurrent quantum yields obtained with porphyrin sensitizers increase as the dye ground-state oxidation potential becomes more anodic, as shown in Figure 10; meanwhile, in the case of P_{Zn} and P, electron injection yields are high and nearly equal. Likewise, Tachibana et al.¹⁹ measured similar and very fast electron injection into TiO₂ from free-base and Zn(II)-tetracarboxyphenyl porphyrin, but they found that the recombination kinetics for the free-base dye is approximately 8-fold slower than that of the metallized one, which would be in agreement with our observation of lower photocurrent quantum yield in

P_{Zn} in comparison with that of P. Thus, it is possible that, as in the case of ruthenium and osmium polypyridyl complexes,^{20–22} the charge recombination rates in ITO/SnO₂/P_M photoelectrodes occur in the Marcus inverted region. However, Clifford et al.¹⁸ also analyzed the molecular control of recombination dynamics in dye-sensitized nanocrystalline TiO₂ films and found an excellent correlation between k_{et} and the spatial separation for a series of ruthenium bipyridyl dyes, showing the importance of this factor and its implications in the design of the sensitizer for dye-sensitized solar cells. In the present case, the studied porphyrins that produce an observable photoelectric effect are expected to be bound to the electrode surface through the peripheral carboxylate ligand, with the dye cation orbital delocalized over the conjugated macrocycle. The change of the central metal affects the orbital distribution in the porphyrins⁶² and probably the distance to the surface, and this cannot be ruled out as a possible factor that influences the electron-transfer rate. The data we present here show a variation of k_b that is less than one decade over 250 mV of variation in E_{ox} , and this seems to be low for accounting for it only in terms of the match of semiconductor and dye energy levels in the Marcus model.

Conclusions

The quantum yields of sensitized photocurrent generation in nanocrystalline SnO₂ thin films with metalloporphyrins have been shown to be highly dependent on the identity of the central metal. Free-base porphyrin and its metal complexes with Zn(II), Cu(II), Pd(II), Ni(II), and Co(II) have been compared in the spectral sensitization of wide band gap semiconductor particles. The SnO₂ films modified only with P_{Zn}, P, P_{Cu}, and P_{Pd} porphyrin dyes exhibit a photoresponse in the visible region, and the close match between the photocurrent action spectrum and the absorption spectrum show that the photosensitization mechanism is operative in extending the photocurrent response of ITO/SnO₂/dye electrode to the visible region.

In the case of P_{Zn} and P, electron injection yields were observed to be high and nearly equal, as has been already reported for similar molecular systems.¹³ This fact would indicate that, in the present case, electron injection yield is not the main cause of the difference observed in the $\Phi_{inj}\eta_c$ product for the different porphyrins.

Photocurrent quantum yields increase as the dye ground-state oxidation potential (E_{ox}) becomes more anodic in both the ITO/SnO₂/dye and ITO/LB electrodes. Laser flash photolysis experiments showed that the back electron-transfer rates decrease with the increase in the driving force for the recombination process, indicating that electron recombination to the oxidized dye probably occurs in the Marcus inverted region, affecting the observed photocurrent quantum yield. This effect could be exploited as a design element in the development of new and better sensitizers for high-efficiency solar cells involving porphyrins and related dyes. Under the present experimental condition, the formation of a metal complex with palladium produces a considerable increase in the photocurrent quantum yield with respect to the widely used free-base and Zn(II) porphyrins.

On the other hand, in the case of porphyrins where the oxidation process is dominated by the metal-centered reaction (Co(II)) or presents valence tautomerism (Ni(II)) it could be possible that there exists a very fast charge recombination between the photoinjected electrons and the M(III)-complex cation that precludes photocurrent generation. However, inefficient electron injection due to the very short lifetime originated

from the π and d orbital interactions could be also the origin of the lack of photocurrent effects in P_{Co^-} and P_{Ni} -sensitized electrodes.

Acknowledgment. We are grateful to Consejo Nacional de Investigaciones Científicas y Técnicas (CONICET-Argentina), Agencia Nacional de Promoción Científica y Tecnológica (ANPCYT-Argentina), Secretaría de Ciencia y Técnica de la Universidad Nacional de Río Cuarto (SECYT-UNRC), and Fundación Antorchas for financial support. L.O., E.N.D., F.F., and J.J.S. are scientific members of CONICET. M.G. thanks CONICET for a research fellowship. Thanks are also due to Professor Previtali for his help in the laser flash photolysis experiments.

References and Notes

- O'Regan, B.; Grätzel, M. *Nature* **1991**, *353*, 737.
- McConnell, R. D. *Renewable Sustainable Energy Rev.* **2002**, *6*, 271.
- Argazzi, R.; Iha, N. Y. M.; Zabri, H.; Odobel, F.; Bignozzi, C. A. *Coord. Chem. Rev.* **2004**, *248*, 1299.
- Memming, R. *Comprehensive Treatise of Electrochemistry*; Plenum Press: New York, 1983; Chapter 7, p 529.
- Gerischer, H.; Willig, F. *Top. Curr. Chem.* **1976**, *61*, 31.
- Hagfeld, A.; Grätzel, M. *Chem. Rev.* **1995**, *95*, 49.
- Kay, A.; Grätzel, M. *J. Phys. Chem.* **1993**, *97*, 6272.
- Otero, L.; Osora, H.; Li, W.; Fox, M. A. *J. Porphyrins Phthalocyanines* **1998**, *2*, 123.
- Campbell, W. M.; Burrell, A. K.; Officer, D. L.; Jolley, K. W. *Coord. Chem. Rev.* **2004**, *248*, 1363.
- Fungo, F.; Otero, L.; Borsarelli, C. D.; Durantini, E. N.; Silber, J. J.; Sereno, L. *J. Phys. Chem. B* **2002**, *106*, 4070.
- Fungo, F.; Otero, L.; Sereno, L.; Silber, J. J.; Durantini, E. N. *J. Mater. Chem.* **2000**, *10*, 645.
- Fungo, F.; Otero, L.; Durantini, E. N.; Silber, J. J.; Sereno, L. E. *J. Phys. Chem. B* **2000**, *104*, 7644.
- Gervaldo, M.; Fungo, F.; Milanesio, M. E.; Otero, L.; Durantini, E. N.; Silber, J. J.; Sereno, L. E. *J. Argent. Chem. Soc.* **2003**, *91*, 153.
- Milanesio, M. E.; Gervaldo, M.; Otero, L.; Sereno, L. E.; Silber, J. J.; Durantini, E. N. *J. Phys. Org. Chem.* **2002**, *15*, 844.
- Milanesio, M. E.; Gervaldo, M.; Otero, L.; Sereno, L.; Silber, J. J.; Durantini, E. N. *J. Porphyrins Phthalocyanines* **2003**, *7*, 42.
- Gervaldo, M.; Otero, L.; Milanesio, M. E.; Durantini, E. N.; Silber, J. J.; Sereno, L. *Chem. Phys.* **2005**, *312*, 97.
- Wang, Q.; Campbell, W. M.; Bonfantani, E. E.; Jolley, K. W.; Officer, D. L.; Walsh, P. J.; Gordon, K.; Humphry-Baker, R.; Nazeeruddin, M. K.; Grätzel, M. *J. Phys. Chem. B* **2005**, *109*, 15397.
- Clifford, J. N.; Palomares, E.; Nazeeruddin, M. K.; Grätzel, M.; Nelson, J.; Li, X.; Long, N. J.; Durrant, J. R. *J. Am. Chem. Soc.* **2004**, *126*, 5225.
- Tachibana, Y.; Haque, S. A.; Mercer, I. P.; Durrant, J. R.; Klug, D. R. *J. Phys. Chem. B* **2000**, *104*, 1198.
- Kuciauskas, D.; Freund, M. S.; Gray, H. B.; Winkler, J. R.; Lewis, N. S. *J. Phys. Chem. B* **2001**, *105*, 392.
- Marcus, R. A. *J. Chem. Phys.* **1965**, *43*, 679.
- Dang, X.; Hupp, J. T. *J. Am. Chem. Soc.* **1999**, *121*, 8399.
- Dolphin, D. *The Porphyrins*; Academic Press: London, 1978.
- Ma, T.; Inoue, K.; Yao, K.; Noma, H.; Shuji, T.; Abe, E.; Yu, J.; Wang, X.; Zhang, B. *J. Electroanal. Chem.* **2002**, *537*, 31.
- Ma, T.; Inoue, K.; Noma, H.; Yao, K.; Abe, E. *J. Photochem. Photobiol., A* **2002**, *152*, 207.
- Bard, A. J.; Faulkner, L. R. *Electrochemical Methods, Fundamentals and Applications*; John Wiley & Sons: New York, 1980.
- Scalise, I.; Durantini, E. N. *J. Photochem. Photobiol., A* **2004**, *162*, 105.
- Watson, D. F.; Marton, A.; Stux, A. M.; Meyer, G. J. *J. Phys. Chem. B* **2004**, *108*, 11680.
- Borsarelli, C. D.; Cosa, J. J.; Previtali, C. M. *Photochem. Photobiol.* **1998**, *68*, 438.
- Haque, S. A.; Tachibana, Y.; Willis, R. L.; Moser, J. E.; Grätzel, M.; Klug, D. R.; Durrant, J. R. *J. Phys. Chem. B* **2000**, *104*, 538.
- Kadish, K. L.; Smith, K. M.; Guillard, R. *The Porphyrin Handbook*; Academic Press: New York, 1999; Vol. 8.
- Truxillo, L. A.; Davis, D. G. *Anal. Chem.* **1975**, *47*, 2260.
- Seth, J.; Palaniappan, V.; Bocian, D. F. *Inorg. Chem.* **1995**, *34*, 2201.
- Kadish, K. M.; Lin, M.; Caemelbecke, E. V.; De Stefano, G.; Medforth, C. J.; Nurco, D. J.; Nelson, N. Y.; Krattinger, B.; Muzzi, C. M.; Jaquinod, L.; Xu, Y.; Shyr, D. C.; Smith, K. M.; Shelnutt, J. A. *Inorg. Chem.* **2002**, *41*, 6673.
- Kadish, K. M.; Morrison, M. M. *J. Am. Chem. Soc.* **1976**, *98*, 3326.
- Kadish, K. M.; Morrison, M. M. *Inorg. Chem.* **1976**, *15*, 980.
- Kadish, K. M.; Morrison, M. M. *Bioinorg. Chem.* **1977**, *7*, 107.
- Walker, F. A.; Beroiz, D.; Kadish, K. M. *J. Am. Chem. Soc.* **1976**, *98*, 3484.
- Bull, R. A.; Bulkowski, J. E. *J. Colloid Interface Sci.* **1983**, *92*, 1.
- Petty, M. C. Molecular Engineering Using the Langmuir-Blodgett Technique. In *Polymer Surfaces and Interfaces*; Feast, W. J., Munro, H. S., Eds.; John Wiley & Sons: New York, 1987; p 163.
- Ogi, T.; Ohkita, H.; Ito, S.; Yamamoto, M. *Thin Solid Films* **2002**, *415*, 228.
- Smith, K. M. General Features of the Structure and Chemistry of Porphyrin Compounds. In *Porphyrins and Metalloporphyrins*; Falk, J. E., Ed.; Elsevier: Amsterdam, 1975; Chapter 1, pp 20–27.
- Choudhury, B.; Weedon, A. C.; Bolton, J. R. *Langmuir* **1998**, *14*, 6192.
- Dick, H. A.; Bolton, J. R.; Picard, G.; Munger, G.; Leblanc, R. M. *Langmuir* **1988**, *4*, 133.
- Kajiwara, T.; Hashimoto, K.; Kawal, T.; Sakata, T. *J. Phys. Chem.* **1982**, *86*, 4516.
- Sakata, T.; Hashimoto, K.; Hiramoto, M. *J. Phys. Chem.* **1990**, *94*, 3040.
- Bedja, I.; Hotchandani, S.; Kamat, P. V. *J. Phys. Chem.* **1994**, *98*, 4133.
- Hashimoto, K.; Hiramoto, M.; Sakata, T. *J. Phys. Chem.* **1988**, *92*, 4272.
- Bisquert, J.; Zaban, A.; Salvador, P. *J. Phys. Chem. B* **2002**, *106*, 8774.
- Bisquert, J.; Zaban, A.; Greenshtein, M.; Mora-Sero, I. *J. Am. Chem. Soc.* **2004**, *126*, 13550.
- Graziani Garcia, C.; Kleverlaan, J.; Bignozzi, C. A.; Iha, N. Y. M. *J. Photochem. Photobiol., A* **2002**, *147*, 143.
- Graziani Garcia, C.; Nakano, A. K.; Kleverlaan, C. J.; Iha, N. Y. M. *J. Photochem. Photobiol., A* **2002**, *151*, 165.
- Zamyatin, A. V.; Gusev, A. V.; Rodgers, M. A. *J. Am. Chem. Soc.* **2004**, *126*, 15934.
- Rodriguez, J.; Kirmaier, C.; Holten, D. *J. Am. Chem. Soc.* **1989**, *111*, 6500.
- Rodriguez, J.; Kirmaier, C.; Holten, D. *J. Chem. Phys.* **1991**, *94*, 6020.
- Yu, Z.; Baskin, J. S.; Steiger, B.; Wan, C. Z.; Anson, F. C.; Zewail, A. H. *Chem. Phys. Lett.* **1998**, *293*, 1.
- Tachibana, Y.; Nazeeruddin, M. K.; Grätzel, M.; Klug, D. R.; Durrant, J. R. *Chem. Phys.* **2002**, *285*, 127.
- Benkö, G.; Myllyperkiö, P.; Pan, J.; Yartsev, A. P.; Sundström, J. *Am. Chem. Soc.* **2003**, *125*, 1118.
- Vlachopoulos, P.; Liska, P.; Augustynski, J.; Grätzel, M. *J. Am. Chem. Soc.* **1988**, *110*, 1216.
- Choudhury, B.; Weedon, A. C.; Bolton, J. R. *Langmuir* **1998**, *14*, 6199.
- Boschloo, G.; Hagfeldt, A. *Chem. Phys. Lett.* **2003**, *370*, 381.
- Rogers, J. E.; Nguyen, K. A.; Hufnagle, D. C.; McLean, D. G.; Su, W.; Gossett, K. M.; Burke, A. R.; Vinogradov, S. A.; Pachter, R.; Fleitz, P. A. *J. Phys. Chem. A* **2003**, *107*, 11331.